Population inference of spin-induced quadrupole moments as a probe for nonblack hole compact binaries

Muhammed Saleem[1,2,*] N. V. Krishnendu[3,4,†] Abhirup Ghosh[5] Anuradha Gupta[6]
W. Del Pozzo[7,8] Archisman Ghosh[9] and K. G. Arun[2,‡]

[1]*School of Physics and Astronomy, University of Minnesota, Minneapolis, Minnesota 55455, USA*
[2]*Chennai Mathematical Institute, Siruseri 603103, Tamilnadu, India*
[3]*Max Planck Institute for Gravitational Physics (Albert Einstein Institute),*
Callinstrasse 38, 30167 Hannover, Germany
[4]*Leibniz Universitat Hannover, D-30167 Hannover, Germany*
[5]*Max Planck Institute for Gravitational Physics (Albert Einstein Institute),*
Am Mühlenberg 1, 14476 Potsdam, Germany
[6]*Department of Physics and Astronomy, The University of Mississippi, Oxford, Mississippi 38677, USA*
[7]*Dipartimento di Fisica "Enrico Fermi", Universita' di Pisa, and INFN sezione di Pisa,*
Pisa I-56127, Italy
[8]*Institute of Gravitational Wave Astronomy, University of Birmingham,*
Edgbaston, Birmingham B15 2TT, United Kingdom
[9]*Ghent University, Proeftuinstraat 86, 9000 Gent, Belgium*

Gravitational wave (GW) measurements of physical effects such as spin-induced quadrupole moments can distinguish binaries consisting of black holes from nonblack hole binaries. While these effects may be poorly constrained for single-event inferences with the second-generation detectors, combining information from multiple detections can help uncover features of nonblack hole binaries. The spin-induced quadrupole moment has specific predictions for different types of compact objects, and a generalized formalism must consider a population where different types of compact objects co-exist. In this study, we introduce a hierarchical mixture-likelihood formalism to estimate the *fraction of nonbinary black holes in the population*. We demonstrate the applicability of this method using simulated GW signals injected into Gaussian noise following the design sensitivities of the Advanced LIGO Advanced Virgo detectors. We compare the performance of this method with a traditionally-followed hierarchical inference approach. Both the methods are equally effective to hint at inhomogeneous populations, however, we find the mixture-likelihood approach to be more natural for mixture populations comprising compact objects of diverse classes. We also discuss the possible systematics in the mixture-likelihood approach, caused by several reasons, including the limited sensitivity of the second-generation detectors, specific features of the astrophysical population distributions, and the limitations posed by the waveform models employed. Finally, we apply this method to the LIGO-Virgo detections published in the second GW transient catalog (GWTC-2) and find them consistent with a binary black hole population with f_{nbh} estimated to be ≤ 0.29 at 90% credibility.

I. INTRODUCTION

Gravitational-wave (GW) observations are slated to unravel a plethora of compact binaries in the coming years. The LIGO-Virgo-KAGRA Collaboration has already reported more than ninety significant detections including binary black holes (BBHs) [1–11], binary neutron stars [12,13] and neutron star–black hole mergers [14],

moreover, this catalogue of events have been updated by several other groups [15–18]. However, one may wonder if there are compact objects other than black holes (BHs) and neutron stars (NSs) that are made of exotic matter or described by some unknown physics.[1] There are theoretical predictions of exotic compact objects which can mimic properties of BHs and are referred as BH mimickers [19,20] (also known as non-BH compact objects). Some examples

---

[*]mcholayi@umn.edu
[†]krnava@aei.mpg.de
[‡]kgarun@cmi.ac.in

[1]White dwarfs, whose sizes are larger than their gravitational radii, are not considered as compact objects in current gravitational wave astronomy.

include boson stars [21–29], fermionic stars [30–35], multicomponent stars [36,37], dark energy stars [38–43] and dark matter stars [36,44–48]. The unknown intrinsic properties of these objects are expected to be imprinted in the GWs they emit and hence GW observations of such objects provide a unique way to probe their presence [49–52].

The compact binary mergers observed by the advanced LIGO [53,54] and the advanced Virgo detectors [55] in the first three observing runs are all consistent with mergers composed of BHs and NSs [2–13,56]. The current sensitivity of detectors is insufficient to rule out the presence of signals from exotic compact objects in the data. With more of such detections in the future [53,57–65], one of the important science goals would be to look for the existence of exotic compact objects in the data [66]. These observations may allow us to constrain what fraction of the detected events could be exotic compact objects. In turn, this can shed light on some of the unexplored physics realms concerning exotic particles and dark matter physics [39,50–52,67–91].

There have been remarkable progress in the modeling of BBH waveforms in the inspiral [92–108], merger [109] and ringdown [110,111] regimes in general relativity (GR). There has also been much progress in modeling binaries containing neutron stars [112–114]. But the same is not true for binaries of BH mimickers, where the progress has been slow, primarily due to the mathematical complications these objects pose in the modeling [51,115–118]. Therefore, looking for the exact imprints of the BH mimicker models in the observed GW signals is difficult.

In the post-Newtonian (PN) formalism, the effects distinguishing BHs from BH mimickers are well studied. These effects include the deformations of the compact objects due to the tidal field of the companion [50,52], or its spinning motion and the effects of tidal heating [84–87]. A number of *tests* have been proposed to distinguish BH mimickers from BHs using parametrizations of such physical effects. Examples include the tests based on the tidal deformability measurements [12,50–52,71–73,78–83,119–121], tidal heating parameter estimations [84–87,122], etc. There are also methods based on the inference of the late-ringdown echo parameters [123].

In this work, we follow a method that uses spin-induced quadrupole moment parameter to distinguish BBHs from binaries of BH mimickers, as outlined in [49,124]. The spin-induced quadrupole moment parameter has a unique value, unity, for Kerr BH according to the no-hair conjecture [125–127], whereas, for any other compact object, its value can be different from unity. A Bayesian framework to measure this parameter has been comprehensively demonstrated in a previous study [66] using simulated GW signals. Moreover, the constraints on the spin-induced quadrupole moment parameters from the GWTC-2 events are reported in [128]. In this work, our focus is on methods

to combine their measurements from *multiple* GW detections, which would be key in enhancing statistical evidence *in favor of* or *against* BH mimickers. In particular, the fact that BHs and BH mimickers can co-exist in the universe, points to the need for having a generic framework that can unravel how various compact objects are distributed in the universe.

We discuss two methods to combine measurements from multiple detections. The first is a so-called *hierarchical combining approach* in which the spin-induced quadrupole moment parameters of the detected population are assumed to follow a Gaussian distribution and use a hierarchical framework to infer the moments of the distribution. A *Gaussian* is among the simplest choices that can approximate a unimodal distribution with just the statistical mean and standard deviation. This approach is similar to the one proposed in [129] and has been used in [130] to infer the distribution of spin-induced quadrupole moment parameters for the LIGO-Virgo detected events. The second method, namely the *mixture-likelihood approach*, explicitly assumes the population to be a mixture of BBH and non-BBH mergers by parametrizing the fraction of events in the respective categories. Specifically, we use a parameter f_{nbh} to quantify the fraction of non-BBH mergers in the detected population. Note that the mixture-likelihood approach is also hierarchical in nature, however, for the sake of name distinction, the notion of *hierarchical* is henceforth used only for the former method.

The applicability of the two approaches are demonstrated using simulated GW signals from binaries of compact objects of diverse classes. The hyperparameters that are used in both the methods can effeciently signal at the non-BH subpopulations that are present in the detected population. Furthermore, the *mixture-likelihood approach* captures the complexity in the population powerfully and can capture the fraction of events that are from non-BH subpopulations. However, some systematics are noticed with the *mixture-likelihood approach*, which could be attributed to the limitations posed by the current detector sensitivities and some of the intrinsic properties of the astrophysical population.

The rest of this paper is organized as follows. We review the GW measurements of spin-induced quadrupole moment parameters in Sec. II. Section III describes the statistical methods employed in this study, including the hierarchical and the mixture-likelihood approaches. In Sec. IV, we detail the properties of simulated population of compact binary mergers used to for this analysis. We discuss the main findings in Sec. V and discuss the systematic effects in Sec. VI. We conclude the study in Sec. VII with a discussion on the future aspects. We also provide an Appendix on how the mixture-likelihood approach would benefit by including astrophysical models of spin-induced quadrupole moments into the framework.

II. REVIEW: GRAVITATIONAL-WAVE MEASUREMENTS OF SPIN-INDUCED MULTIPOLE MOMENTS

The spin-induced multipole moments arise due to the spinning motion of the compact objects in the binary and these effects appear in the gravitational waveform along with the self-spin terms. The leading order effect [49,98,131] at the second post-Newtonian (2PN) order can be schematically represented in the following form,

$$Q = -\kappa \chi^2 m^3, \qquad (1)$$

where Q is the spin-induced quadrupole moment scalar, κ is the spin-induced quadrupole moment parameter, m is the mass and χ is the dimensionless spin parameter, defined as $\vec{\chi} = \vec{S}/m^2$ where $\vec{S}$ is the spin angular momentum of the compact object.

The spin-induced quadrupole moment parameter κ has a unique value, unity, for Kerr BH according to the no-hair conjecture [125–127], whereas, for any other compact object, its value can be different from unity. For example, for spinning NSs, the value of κ varies between $\sim$2–14 depending upon the internal structure of the star [88–90]. Also, calculations show that the value of κ can vary roughly between 10 to 150 for boson stars [28] while for gravastars [132] κ can be negative as well [133,134]. In Fig. 1 we compare gravitational waveforms of BBHs (i.e., $\kappa = 1$) and non-BBHs ($\kappa \neq 1$) for two different values of spin parameters.

Both the binaries have same masses $(m_1, m_2) = (20, 10)\, M_\odot$ while non-BBHs have $(\kappa_1, \kappa_2) = (40, 25)$. Highly spinning binaries have $(\chi_1, \chi_2) = (0.6, 0.5)$ while slowly spinning binaries have $(\chi_1, \chi_2) = (0.15, 0.1)$, assuming the spins aligned to the orbital angular momentum axis. We used `IMRPhenomPv2` [135–137] waveform model to simulate the time-domain GW signal. We see that as the spins of the binary components increase, the dephasing between the BBH and non-BBH waveforms increases.

A Bayesian framework to measure the κ parameters was demonstrated in [66], to constrain the nature of the stellar mass compact binaries detected by Advanced LIGO and Advanced Virgo detectors. It was shown that the spin-induced quadrupole moment measurements can be used to distinguish the observed BBHs from non-BBHs for inspiral dominated systems with moderate to high spins [66].

In this framework, one uses BBH waveforms which allow the spin-induced quadrupole moment coefficient κ to vary around the expected Kerr value as $\kappa = 1 + \delta\kappa$ depending upon the black hole mimicker model assumptions. Here the parametrized deformations (labeled as $\delta\kappa$) represents the deviations from the BH nature. It is pointed out in [66] that the simultaneous measurement of $\delta\kappa_1$ and $\delta\kappa_2$ is difficult due to strong correlations between binary parameters in the gravitational waveform. In order to capture the deviation from the BBH nature Ref. [66] proposed to measure their symmetric combination $\delta\kappa_s = (\delta\kappa_1 + \delta\kappa_2)/2$, assuming the antisymmetric combination $\delta\kappa_a = (\delta\kappa_1 - \delta\kappa_2)/2$ vanishes
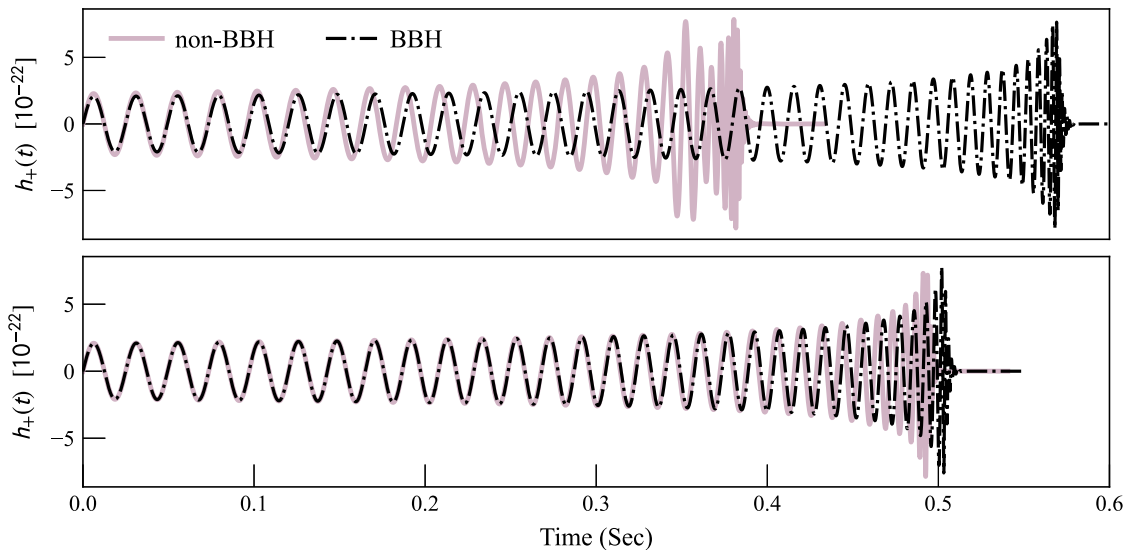
FIG. 1. Time-domain gravitational waveforms for a fast-spinning (top) and slowly-spinning (bottom) compact binary mergers with component masses $(m_1, m_2) = (20, 10)\, M_\odot$. The spins are aligned with the orbital angular momentum vectors (no precession modulations) and have the dimensionless spin magnitudes $(\chi_1, \chi_2) = (0.6, 0.5)$ for the top and $(\chi_1, \chi_2) = (0.15, 0.1)$ for the bottom panels. The black (dash-dot) traces are BBH waveforms, and the red (solid) traces are non-BBH waveforms with spin-induced quadrupole moment parameters assuming $\delta\kappa_1 = 40$ and $\delta\kappa_2 = 25$ for component compact objects. The time-domain waveforms are generated using backward fast Fourier transform (FFT) of the frequency-domain waveform model, `IMRPhenomPv2`. For each waveform, the time t (x axis) is set to zero at a point when the instantaneous frequency of the waveform is 40 Hz, and the waveforms are also aligned to be in phase at that point.

for a BBH signal. The $\delta\kappa_a = 0$ assumption also implies that the individual compact objects in the binary system are of the same nature. For cases with any violation of this assumption, we would expect an offset in $\delta\kappa_s$ posterior distribution, and such cases need more investigations keeping $\delta\kappa_1$ and $\delta\kappa_2$ as separate parameters. (See [124] for a more detailed discussion). The applicability of this test has been further explored in the context of expected detections from the third generation GW detectors [138].

III. FORMALISM

In a universe where all the massive compact objects are BBHs, $\delta\kappa_s$ assumes the unique and universal value $\delta\kappa_s = 0$. However, if we admit the possibility that compact objects come in many flavors, this universality assumption would be wrong, and the inference on $\delta\kappa_s$ obtained by naively multiplying each observation's likelihood would lead to erroneous conclusions. Even for the binaries that are made up of some specific class of exotic compact objects with a unique equation of state, the value of $\delta\kappa_s$ could vary depending on the intrinsic properties such as masses and spins as is found to be the case for boson stars [28]. In such a case where the value of $\delta\kappa_s$ can vary from event to event, one would aim to infer the underlying distribution of $\delta\kappa_s$ associated with the compact binary population. This is the context in which we discuss the two combining approaches and their applicability.

Below, we introduce our notations for the Bayesian inference variables, followed by the formalisms for hierarchical combining and mixture-likelihood approach.

A. Bayesian inference: Basic notations

The first step in our formalism is to perform the Bayesian parameter estimation of all the detected GW events. Here, we briefly overview the Bayesian inference method employed to estimate the spin-induced quadrupole moment parameter, $\delta\kappa_s$. We define $\vec{\theta}$ as the vector representing the set of parameters that describes a BBH merger on quasi-circular orbits. This includes masses, spins, luminosity distance, time and phase of arrival, and the angles describing the sky-location and binary orientation. The data from the jth event is labeled as d_j, and the set of data from N events together is denoted as $\vec{d}$. $\mathcal{H}$ is our hypothesis that the data d_j carries a signal $h_j(\vec{\theta}, \delta\kappa_s)$ plus colored Gaussian random noise. Under this hypothesis, the posterior for the binary parameters can be written as,

$$p(\vec{\theta}, \delta\kappa_s | d_j, \mathcal{H}) = \frac{\pi(\vec{\theta}, \delta\kappa_s | \mathcal{H}) \mathcal{L}(d_j | \vec{\theta}, \delta\kappa_s, \mathcal{H})}{\mathcal{Z}_j^{nbh}}, \quad (2)$$

where $\mathcal{L}(d_j | \vec{\theta}, \delta\kappa_s, \mathcal{H})$ is the likelihood of d_j being the data given the parameters $\{\vec{\theta}, \delta\kappa_s\}$, and $\pi(\vec{\theta}, \delta\kappa_s | \mathcal{H})$ is the prior probability of parameters $\{\vec{\theta} \cdot \delta\kappa_s\}$. The evidence

$\mathcal{Z}_j^{nbh} = P(d_j | \mathcal{H})$ is obtained by marginalizing the likelihood over the prior,

$$\mathcal{Z}_j^{nbh} = \int \pi(\vec{\theta}, \delta\kappa_s) \mathcal{L}(d_j | \vec{\theta}, \delta\kappa_s) d\vec{\theta} d\delta\kappa_s, \quad (3)$$

where, the superscript *nbh* stands for the non-BBH hypothesis and we have dropped $\mathcal{H}$ for brevity. The BBH hypothesis is a special case obtained by fixing $\delta\kappa_s = 0$ in the likelihood $\mathcal{L}(d_j | \vec{\theta}, \delta\kappa_s = 0)$ which we simply write as $\mathcal{L}(d_j | \vec{\theta})$ and the corresponding evidence can be expressed as,

$$\mathcal{Z}_j^{bh} = \int \pi(\vec{\theta}) \mathcal{L}(d_j | \vec{\theta}) d\vec{\theta}. \quad (4)$$

The posterior on $\delta\kappa_s$ can be obtained by marginalizing Eq. (2) over the BBH parameters as

$$p(\delta\kappa_s | d_j, \mathcal{H}) = \int p(\vec{\theta}, \delta\kappa_s | d_j, \mathcal{H}) d\vec{\theta}. \quad (5)$$

The `IMRPhenomPv2` signal model [135–137] used for the Bayesian analysis includes $\delta\kappa_s$ as a free parameter along with the BBH parameters $\vec{\theta}$. We assume a uniform prior on $\delta\kappa_s$ in $[-500, 500]$. For the component masses, we consider uniform priors on in the range $[4, 100]\ M_\odot$. The priors on component spin-magnitudes are uniform in $[0,1]$ and their orientations assumed to be isotropic. We choose the luminosity distance prior to be uniform in comoving volume ranging between $[10, 5000]$ Mpc. The parameter estimation is performed using the `lalinference_nest` sampler available in the `LALInference` library package [139]. The posterior samples as well as the Bayesian evidences in Eq. (3) and (4) are obtained as raw outputs from `lalinference_nest`.

Below, we discuss the two different approaches for combining $\delta\kappa_s$ measurements from the Bayesian analysis of individual events.

B. Hierarchical combining approach: Population distribution of $\delta\kappa_s$

In this approach, we assume that $\delta\kappa_s$ follows some underlying distribution governed by a set of hyperparameters $\vec{\alpha}$, similar to the method demonstrated in [129]. The posterior on $\vec{\alpha}$ given the data $\vec{d}$ can be written as

$$p(\vec{\alpha} | \vec{d}) \propto \mathcal{L}(\vec{d} | \vec{\alpha}) p(\vec{\alpha}), \quad (6)$$

where the proportionality becomes equality by normalizing the right-hand side to unity. The prior $p(\vec{\alpha})$ is taken to be flat assuming no prior knowledge of the underlying distribution of the hyperparameters $\vec{\alpha}$. Here $\mathcal{L}(\vec{d} | \vec{\alpha})$ is the

likelihood function which can be obtained as a product of likelihoods of $\vec{\alpha}$ from individual events, as

$$\mathcal{L}(\vec{d}|\vec{\alpha}) = \prod_{j=1}^{N} \mathcal{L}(d_j|\vec{\alpha}). \qquad (7)$$

which can be further expanded by rewriting the likelihood for the jth event as a marginalization over the $\delta\kappa_s$ parameter,

$$\mathcal{L}(\vec{d}|\vec{\alpha}) = \prod_{j=1}^{N} \left[\int \mathcal{L}(d_j|\delta\kappa_s) p(\delta\kappa_s|\vec{\alpha}) d\delta\kappa_s \right]. \qquad (8)$$

In the above equation, the term $\mathcal{L}(d_j|\delta\kappa_s)$ in the integral is the likelihood of $\delta\kappa_s$ for the jth event, marginalized over the BBH parameters. Since we use a uniform prior on $\delta\kappa_s$ in the single-event analyses, this likelihood will be the same as the posterior given in Eq. (5). The other term in the integral of Eq. (8), $p(\delta\kappa_s|\vec{\alpha})$ is the predicted distribution of $\delta\kappa_s$ given the hyperparameters $\vec{\alpha}$. In this study, as mentioned earlier, we assume a Gaussian distribution with hyperparameters $\vec{\alpha} = \{\mu, \sigma\}$ which implies to,

$$p(\delta\kappa_s|\vec{\alpha}) = \mathcal{N}(\mu, \sigma^2). \qquad (9)$$

In this study, we assume μ and σ to have uniform priors in the ranges $[-150, 150]$ and $[0, 300]$ respectively and we use the `Dynesty` sampler from `Bilby` to sample over μ and σ as per the likelihood given in Eq. (8).

Once the posterior of μ and σ (or $\vec{\alpha}$ in general) is computed, the population distribution of $\delta\kappa_s$ can be obtained as,

$$p(\delta\kappa_s|\vec{d}) = \int p(\delta\kappa_s|\vec{\alpha}) p(\vec{\alpha}|\vec{d}) d\vec{\alpha}, \qquad (10)$$

where we have marginalized $\delta\kappa_s$ over the inferred distributions of the hyperparameters $\vec{\alpha}$.

C. Mixture-likelihood approach: Estimating the fraction of non-BBH events

Unlike the hierarchical approach in the preceding section, here we ask a more generic question "what *fraction* of the detected population are from non-BBH events?". We try to answer this with a *mixture-likelihood* which parametrizes the presence of non-BBH events as f_{nbh}, defined as the *fraction* of total detected signals that are from non-BBH events. Mixture likelihoods have been used in literature for various problems, see e.g., Ref. [140].

Let us start with the single-event likelihood expression for the non-BBH model,

$$\mathcal{L}(d_j|\vec{\theta}, \delta\kappa_s) \propto \exp\left(-\frac{1}{2}(d_j - h_j(\vec{\theta}, \delta\kappa_s)|d_j - h_j(\vec{\theta}, \delta\kappa_s))\right). \qquad (11)$$

Here $(|)$ represents the noise-weighted inner product, defined as $(x|y) = 4\Re \int_0^\infty x(f)^* y(f)/S_n(f) df$, where the $*$ indicates complex conjugate and $S_n(f)$ is the one-sided power spectral density (PSD) of the noise. Suppose a fraction f_{nbh} of the overall detectable signals are from non-BBH events, then the probability of any single event being a non-BBH will be equal to f_{nbh}. On the complementary side, the probability of any event being a BBH will be equal to $(1 - f_{nbh})$, as BBH and non-BBH are two mutually exclusive and exhaustive[2] cases. To take into account these possibilities, we can rewrite the likelihood as a sum of the BBH and non-BBH likelihoods weighted by their respective probabilities as

$$\mathcal{L}(d_j|\vec{\theta}, \delta\kappa_s, f_{nbh}) = (1 - f_{nbh})\mathcal{L}(d_j|\vec{\theta}) + f_{nbh}\mathcal{L}(d_j|\vec{\theta}, \delta\kappa_s). \qquad (12)$$

Equation (12) is the single-event mixture-likelihood. Marginalizing over $\vec{\theta}$ and $\delta\kappa_s$, the above expression becomes,

$$\mathcal{L}(d_j|f_{nbh}) = (1 - f_{nbh}) \times \int \pi(\vec{\theta})\mathcal{L}(d_j|\vec{\theta}) d\vec{\theta}$$
$$+ f_{nbh} \times \int \pi(\vec{\theta}, \delta\kappa_s)\mathcal{L}(d_j|\vec{\theta}, \delta\kappa_s) d\vec{\theta} d\delta\kappa_s, \qquad (13)$$

where the integrals on the rhs are the evidences for the BBH and non-BBH models, defined in Eq. (4) and (3). Equation (12) then becomes,

$$\mathcal{L}(d_j|f_{nbh}) = (1 - f_{nbh})\mathcal{Z}_j^{bh} + f_{nbh}\mathcal{Z}_j^{nbh}. \qquad (14)$$

Note that in going from Eq. (13) to Eq. (14), we have used a uniform prior on $\delta\kappa_s$ as described in Sec. III A. In Sec. VI, we will investigate how the prior choices would affect the results.

For a population of N detected events, the combined likelihood can be written as,

$$\mathcal{L}^{pop}(\vec{d}|f_{nbh}) = \prod_{j=1}^{N} ((1 - f_{nbh})\mathcal{Z}_j^{bh} + f_{nbh}\mathcal{Z}_j^{nbh}). \qquad (15)$$

Equation (15) is the *mixture-likelihood* for a population and can be evaluated for any value of f_{nbh}, by only knowing the

---

[2]Alternatively, one can consider specific non-BH models such as boson stars and/or gravastars. However, these models, together with the BH model, would still be nonexhaustive as yet unknown non-BH models could possibly exist.

evidences of BBH and non-BBH models for all the events in the population. With the above likelihood evaluated, we can express the posterior on f_{nbh} as,

$$p(f_{\text{nbh}}|\vec{d}) \propto \pi(f_{\text{nbh}})\mathcal{L}^{\text{pop}}(\vec{d}|f_{\text{nbh}}), \qquad (16)$$

where the prior on f_{nbh} can be taken as uniform, $\mathcal{U}(0,1)$ owing to the most generic and uninformative case.

Additionally, one can also define three mutually exclusive population-hypotheses based on the f_{nbh} values.

(1) $f_{\text{nbh}} = 0$: "all the events are BBHs,"
(2) $0 < f_{\text{nbh}} < 1$: "the population is a mixture of BBH and non-BBH events,"
(3) $f_{\text{nbh}} = 1$: "all the events are non-BBHs."

It is straightforward to compute the Bayes factors between any of these two hypotheses. The Bayes factor between "all are BBH" and "mixture of BBH and non-BBH events" can be obtained as

$$\mathcal{B}_{\text{mix}}^{BBH} = \frac{\mathcal{L}^{\text{pop}}(\vec{d}|f_{\text{nbh}} = 0)}{\int_{0 < f_{\text{nbh}} < 1} \mathcal{L}^{\text{pop}}(\vec{d}|f_{\text{nbh}})\pi(f_{\text{nbh}})\mathrm{d}f_{\text{nbh}}}, \quad (17)$$

where the denominator included marginalizing the likelihood in Eq. (15) over the relevant range of f_{nbh}. Similarly, the Bayes factor between "all are BBH" and "all are non-BBH" events can be obtained as,

$$\mathcal{B}_{non-BBH}^{BBH} = \frac{\mathcal{L}^{\text{pop}}(\vec{d}|f_{\text{nbh}} = 0)}{\mathcal{L}^{\text{pop}}(\vec{d}|f_{\text{nbh}} = 1)}. \qquad (18)$$

IV. SIMULATED COMPACT BINARY POPULATION

To demonstrate the performance of different combining approaches, we simulate a set of compact binary populations that include only BBH signals, only non-BBH signals, and different types of mixtures that include BBH and non-BBH signals at different proportions. In the subsections below, we describe the steps we followed to construct the populations.

A. Masses and spins

(1) We first choose a representative mass model from which we draw the component masses. The primary masses (m_1) follow a distribution what is referred to as *Model-C* in [141] which is a power-law function smoothed at the lower mass end and embedded with a Gaussian peak toward the higher mass end. The secondary masses (m_2) are drawn from a smoothed power-law conditional on the primary masses such that $m_1 \geq m_2$.

(2) For each binary, the magnitudes of the two component-spins are drawn according to the *Default Model* as named in [142]. In this model, the spin

magnitudes a_i ($i = 1, 2$) are drawn from a beta distribution

$$p(a_i|\alpha_a,\beta_a) \propto a_i^{\alpha_a-1}(1 - a_i^{\beta_a-1}), \qquad (19)$$

where α_a and β_a are shape parameters. We choose $\alpha_a = 2.75$ and $\beta_a = 6.00$ to make sure that we do not have sources with $a_i \sim 0$, as nonspinning compact objects do not carry imprints of spin-induced multipole moments.

(3) The spin orientations are randomly drawn from a mixture of *isotropic* and *aligned-to-orbital-angular-momentum* orientations. In other words, the populations include binaries with precessing spins and binaries with nonprecessing spins.

Note that there are several mass and spin models in literature [142] which can explain the current GW data, and our choice here is arbitrary since they do not affect the conclusions of this study.

B. Source selection based on signal-to-noise-ratio

The sources with masses and spins as described above are distributed uniformly in comoving volume up to a redshift of 0.5 [8,142]. The inclination and polarization angles are chosen so that the binary orientations are isotropically distributed with respect to detectors.

We construct our populations from sources that pass the following two criteria:

$$\text{SNR} \geq 10,$$
$$\text{SNR}_{\text{insp}} \geq 2\,\text{SNR}_{\text{post-insp}}, \qquad (20)$$

where, SNR is the optimal network signal-to-noise ratio with the HLV network, assuming all of them at their designed sensitivity [55,143–145]. SNR_{insp} and $\text{SNR}_{\text{post-insp}}$ are the signal-to-noise ratio in the inspiral and post-inspiral (merger-ringdown) regimes of the signal, respectively, determined by an inspiral cutoff frequency given by the inspiral to intermediate transition frequency of phenomenological waveform models. This cut-off frequency is calculated, given the total mass of the binary (M) as, $f_{\text{cut}} = 0.018/M$ [135–137].

The second criterion imposes the inspiral SNR to be at least twice the postinspiral SNR, which makes sure that there are enough number of waveform cycles in the inspiral phase. This is because the spin-induced quadrupole moment effects predominantly affect the inspiral phase, as modeled in the current waveform models. However, with the advancements in numerical relativity simulations, future waveform models might accurately account for their evolution in the post-inspiral phase, which in turn would allow us to test *higher-mass* binaries whose SNR dominates in the post-inspiral phase.

C. Distribution of spin-induced quadrupole moment parameters

We simulate six random instances of the BBH populations with parameters as described in the preceding sections and apply the SNR criterion of Eq. (20). We keep the first of these as a BBH population but turn the other five into either a non-BBH or a mixture population by associating spin-induced quadrupole moment parameters ($\delta\kappa_1$ and $\delta\kappa_2$) to each of them. Addition of these parameters would in principle change the SNR of the signals, however, the changes in our case are small[3] ($\lesssim 3\%$) and all the signals still survive the SNR criterion.

The $\delta\kappa_1$ and $\delta\kappa_2$ distributions for every populations are made by mixing three components: a uniform distribution $\mathcal{U}(-40, 40)$ (Uniform), a positive Gaussian with a mean value 25 and standard deviation of 5, $\mathcal{N}(25, 5^2)$ (GausPos), and a similar Gaussian with a negative mean, $\mathcal{N}(-25, 5^2)$ (GausNeg). We chose a few representative values for the mixing proportions and the total number of sources for the various populations. The boundaries of the uniform distribution or the mean and variance of the two Gaussian distributions do not carry any direct physical significance, rather these are chosen for the sake of diversity in the non-BBH signals.

All the six populations and their $\delta\kappa_1$ and $\delta\kappa_2$ distributions are summarized in Table I. Note that we do not impose $\delta\kappa_1 = \delta\kappa_2$ (or $\delta\kappa_a = 0$) for the simulated signals, to keep them as generic as possible, though our analysis framework makes this assumption. In general, the compact binary distribution in the universe could be diverse, characterized by different values of $\delta\kappa_s$ and $\delta\kappa_a$. We create various population models to mimic such scenarios by allowing the fraction of non-BBH systems to differ from model to model. We list all the six population below. You may refer to Table I for the details of their ingredients.

(1) BBH: A fully BBH population.
(2) NonBBH: A fully non-BBH population with $\delta\kappa_1$ and $\delta\kappa_2$ drawn from Uniform, GausPos and GausNeg.
(3) NonBBHPos: A fully non-BBH population with $\delta\kappa_1$ and $\delta\kappa_2$ taking only positive values, i.e., from GausPos and Uniform with a restriction that $\delta\kappa_{1,2} > 10$.
(4) NonBBHNeg: A fully non-BBH population with $\delta\kappa_1$ and $\delta\kappa_2$ taking only negative values, i.e., from GausNeg and Uniform with a restriction that $\delta\kappa_{1,2} < -10$.
(5) MixtureAll: A population containing 50% BBH signals and 50% non-BBH signals whose $\delta\kappa_1$ and $\delta\kappa_2$ are drawn from Uniform, GausPos and GausNeg.

---

[3]Due to the moderate to low spin values of the sources in our populations, we do not expect the power in the signals to change significantly, which is also apparent in the bottom panel of Fig. 1.

TABLE I. Details of the simulated compact-binary populations used in this study. Our six populations are labelled as written in the left-most column. The second column provides the fraction (f_{nbh}) of non-BBH signals contained in each population. The third column provides the number of BBH signals in each population. The $\delta\kappa_1$ and $\delta\kappa_2$ values of the non-BBH signals in each population are distributed as a mixture of three statistical models: a uniform distribution $\mathcal{U}(-40, 40)$ (Uniform), a positive Gaussian $\mathcal{N}(25, 5^2)$ (GausPos), and a negative Gaussian $\mathcal{N}(-25, 5^2)$ (GausNeg). The columns 4-6 describes respective numbers drawn from each of these model. Finally, the right-most column gives the total size of the population (N_{tot}).

Model	f_{nbh}	BBH	Uniform	GausPos	GausNeg	N_{tot}
BBH	0.0	50	0	0	0	50
NonBBH	1.0	0	20	15	15	50
NonBBHPos	1.0	0	10	15	0	25
NonBBHNeg	1.0	0	10	0	15	25
MixtureAll	0.5	30	10	10	10	60
MixturePos	0.5	20	10	10	0	40

(6) MixturePos: A population containing 50% BBH signals and 50% non-BBH signals whose $\delta\kappa_1$ and $\delta\kappa_2$ are taking only positive values, from GausPos, and Uniform with a restriction that $\delta\kappa_{1,2} > 10$.

We use the IMRPhenomPv2 waveform model [135–137,146] for simulating all the signals, which is the same as the model used for the Bayesian analysis as well, as mentioned before.

V. RESULTS

A. Hierarchical combining approach

We apply the method described in Sec. III B on all the six simulated populations described in Table I. The results are shown as violin plots in Fig. 2. The top two rows (silver) show the posterior distributions of the hyperparameters μ and σ for each population and the bottom panel shows the $\delta\kappa_s$ distributions reconstructed from μ and σ according to Eq. (10). For BBH, the distributions of both μ and σ peak at their true values (i.e., zero) with narrow error bars and so is the $\delta\kappa_s$ distribution which is constrained to $[-10.7, 8.8]$ at 90% credibility. However, this is not the case with the rest of the populations, as we discuss below.

For the NonBBH, the μ posterior is consistent with zero which is expected because it has equal number of sources from both sides of $\delta\kappa_s = 0$. The σ posterior has increasing support toward the higher end of the prior and there is little to no support for $\sigma = 0$. This implies that the population could not be fit with a simple Gaussian and can be taken as an indication to the presence of one or more of subpopulation with different values of $\delta\kappa_s$. The marginalized $\delta\kappa_s$ distribution for this case is a wide distribution with no insight, which results from the behavior of the σ posterior.

For the NonBBHPos and NonBBHNeg, the μ tends to peak at their true values again but the σ posteriors do not
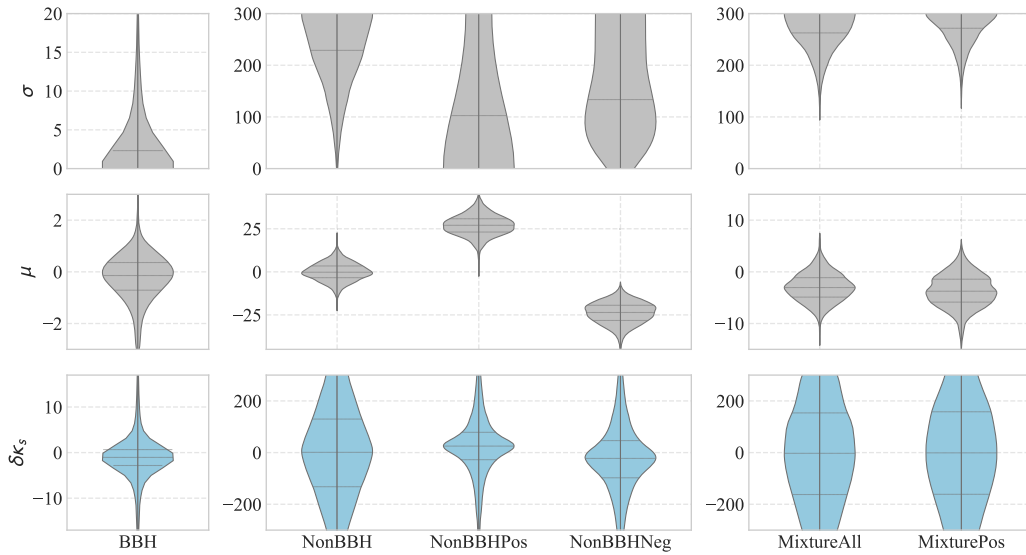
FIG. 2.   Violin plots showing the results from hierarchical combining formalism applied on the six simulated populations as labeled on the x-axis. The top two rows (silver) are the posterior densities of the hyper parameters μ and σ characterising the *Gaussian* that models the population distribution $\delta\kappa_s$ (see Sec. III B and Eq. (9) for details). The bottom row (blue) shows the $\delta\kappa_s$ distributions obtained by marginalizing over the μ and σ posteriors [as per Eq. (10)]. We assumed μ and σ to have uniform priors in the ranges $[-150, 150]$ and $[0, 300]$ respectively and sampled using the `Dynesty` sampler from `Bilby`.

exclude zero. This is because the injected distributions of $\delta\kappa_s$ are one-sided for these two ($\sim [0, 40]$ and $\sim [-40, 0]$) unlike `NonBBH` ($\sim [-40, 40]$) and hence are relatively better candidates for finite-width Gaussians. Furthermore, we see that the peaks of the $\delta\kappa_s$ distributions are shifted to positive and negative values respectively for `NonBBHPos` and `NonBBHNeg`, as one would expect, though they do not exclude zero.

For the mixture populations (`MixtureAll` and `MixturePos`), the σ posteriors completely excludes zero and peaks at the highest value allowed by the prior. This again shows that a Gaussian of finite width could not be used to represent the underlying $\delta\kappa_s$ distribution and hence one could conclude the population to have complex components. The reconstructed $\delta\kappa_s$ distributions are, as expected, uninformative.

In summary, the *hierarchical combining approach* provides reasonably good estimates when we have only BBH signals or only non-BBH signals with all of them belonging to similar nature, i.e., $\delta\kappa_s$ having only positive/ negative values in a small range of values like the ones we considered. For mixture population containing both BBH and non-BBH signals, the method can indicate to the complexity of the underlying distributions however can not realize whether it is full of non-BBH or a mixture of both BBH and non-BBH.

B. Mixture likelihood approach

Now, we apply the *Mixture likelihood* method (Sec. III C) on all the six simulated populations of Table I. Figure 3 shows the posteriors on f_{nbh}, the fraction of non-BBH

events in the population. We see that, for the BBH-only population (`BBH`), the f_{nbh} distribution peaks at zero, as expected. For the non-BBH populations with no BBH sources at all (`NonBBH`, `NonBBHPos` and `NonBBHNeg`), we expect f_{nbh} to peak at unity. However, the peaks occur between 0.1 and 0.5. Similarly, for the mixture populations with an equal number of BBH and non-BBH sources (`MixtureAll` and `MixturePos`), the peaks are expected to be at 0.5, but we obtain the peaks between 0.2 and 0.4.
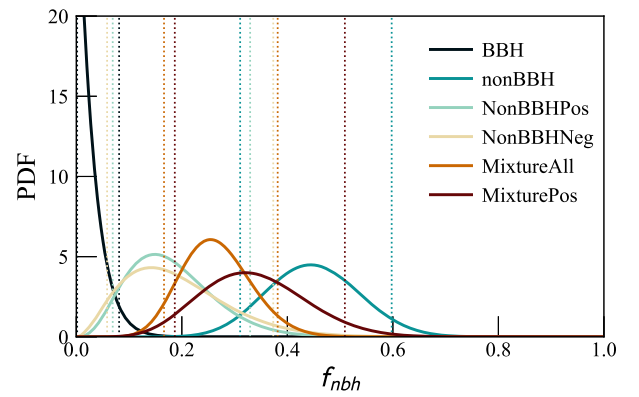
FIG. 3.   Posterior distributions of the f_{nbh} parameter—the fraction of non-BBH signals in the population—estimated using the *mixture-likelihood* approach. For a population with only BBH signals, the posterior is expected to peak at zero. A peak at unity would imply to a population with only non-BBH signals while a peak in between indicating a mixture population with BBH and non-BBH signals. The posteriors shown here are for the six simulated compact binary populations described in Table I. The vertical dashed lines represent the 90% credible intervals.

This shows that there is an overall tendency for f_{nbh} to lean toward the BBH value. These offsets can be understood as systematics due to multiple reasons and have been discussed in detail in Sec. VI. Nevertheless, for all the non-BBH populations we have chosen, the f_{nbh} posteriors exclude zero at 90% credibility.

In Fig. 4, we show the $\log_e$ Bayes factor between the "All BBH" vs the "Mixture of BBH and non-BBH" hypotheses as derived in Eq. (17), as a function of the injected value of f_{nbh}. Note that we do not use any of the populations in Table I for this plot. Rather, we follow an averaging procedure using the sources in all those populations. We first construct two pools of BBH and non-BBH sources by collecting all the available sources from the six populations in Table I. Now, for a given value of f_{nbh} on the x-axis, for example, $f_{nbh} = 0.4$, we randomly pick 12 BBH and 18 non-BBH sources from the respective pools, with a total of 30 sources. By repeating this 500 times, we compute $\log_e$ Bayes factor for all these 500 cases and then compute the median and 68% credible levels which are shown on the y-axis of Fig. 4. The averaging helps remove the fluctuations due to any statistical outliers when considering a population size as small as 30.

The $\log_e$ Bayes factor favors the "only BBH" hypothesis when we inject only BBH signals (at $f_{nbh} = 0$), whereas it rules out the "only BBH" model for all the populations that included non-BBH signals (as we move toward larger values of f_{nbh}). The error bars show that the populations with higher values of f_{nbh} (say > 0.8) can be distinguished
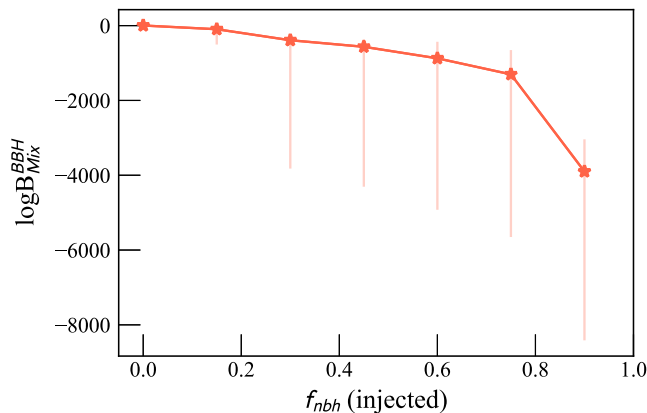
FIG. 4.   Figure showing how the $\log_e$ Bayes factor between the population-hypotheses "All are BBH" and "A mixture of BBH and non-BBH" [as derived in Eq. (17)] varies as a function of the true value of the f_{nbh} of the population. At each f_{nbh} on the x-axis, the y-axis shows the median and 68% error-bars on the log Bayes factor distribution which, in turn, is obtained from 500 population instances, each having $N_{tot} = 30$. The 500 instances are constructed by collecting the simulated events across the six populations of Table I. The ensembles are not mutually exclusive as we have a limited number of sources in the population but help reduce the outlier effects. Furthermore, the huge error bars are a consequence of the population-size being as small as 30 and would definitely improve with the increasing number of sources.

from populations with lower values such as $f_{nbh} < 0.1$ at 68% credibility. For most of the intermediate values of f_{nbh}, there are huge and overlapping error bars on Bayes factors which would be expected for the current population-size and would definitely shrink with the addition of more sources into the population.

C. Estimation of fraction of non-BBH signals from real LIGO-Virgo observations

The first bounds on spin-induced quadrupole moment parameter from observed gravitational wave events are reported in [66]. Furthermore, Ref. [130] provided the combined posterior distributions on $\delta\kappa_s$ obtained from the O1, O2, and the first half of O3 observing runs of LIGO-Virgo detectors along with the individual bounds. In [130], the combined bounds and Bayes factors are calculated following two methods: multiplying likelihoods (universality assumption on $\delta\kappa_s$) and hierarchical combining. Here we demonstrate the applicability of the mixture likelihood approach on all the events considered in [130] and infer f_{nbh} for this population. We use the public data available from [147]. The result is shown in Fig. 5. Our analysis confirms that the detections reported in GWTC-2 [128] are consistent with a BBH population.

VI. UNDERSTANDING THE SYSTEMATIC BIASES

The bias in the f_{nbh} posterior toward the BBH value ($f_{nbh} = 0$) as discussed above and shown in Fig. 3 could be a sum of various effects in play. We discuss these effects in the present section.

A. Biased single-event inferences

One of the possible reasons for the systematic bias in the inference of f_{nbh} is the choices of spins and SNRs of the
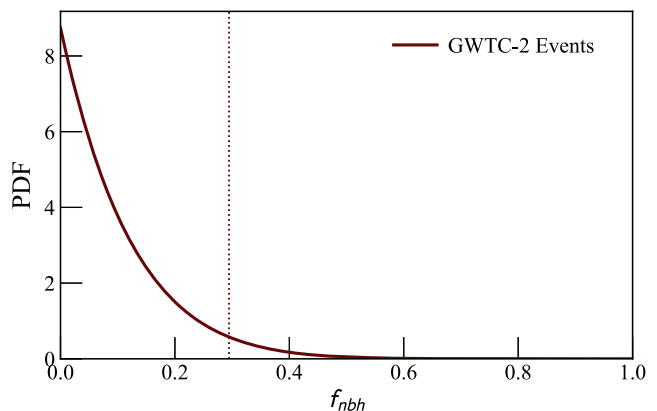
FIG. 5.   Same as Fig. 3 but the posterior of f_{nbh} for the compact binary detections of Advanced LIGO and Advanced Virgo reported in the GWTC-2 considered for testing GR analysis [130]. The peak of the posterior, as obtained here, is consistent with a population of only BBH signals.
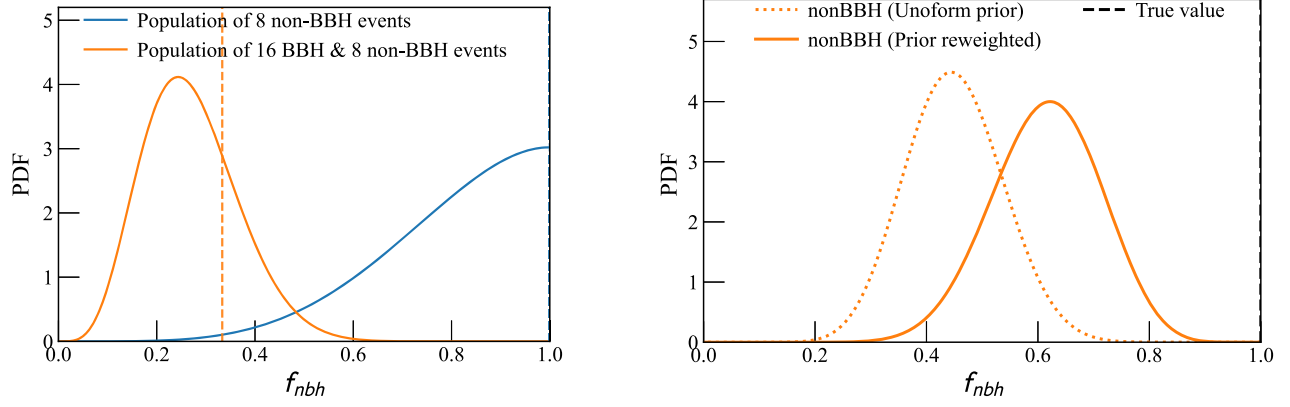
FIG. 6.   Left: posterior distribution of $f_{\rm nbh}$ for populations that include simulated sources with $|\chi_{\rm eff}| \geq 0.15$ and network $SNR_{\rm insp} \geq 20$. These populations are constructed by collecting sources from all the six populations that satisfy the SNR and spin criterion. Right: the posterior distribution on the fraction $f_{\rm nbh}$ with and without prior-reweighting discussed in Sec. VI and Appendix. On both the panels the dashed vertical lines indicate the injected value of $f_{\rm nbh}$.

individual events in the populations. It has been shown that the single-event $\delta\kappa_s$ inferences are better when the spins are higher, and of course, improves further with higher SNR [124] while our populations include many events with low SNRs and low spins.

To investigate this, we collect events from our simulations that have effective spins $|\chi_{\rm eff}| \geq 0.15$ and the network $SNR_{\rm insp} \geq 20$.[4] Out of all the BBH and non-BBH simulations that span over six populations, we obtain 16 BBH and 8 non-BBH events satisfying the above criterion. We construct two populations out of them: (1) All the 8 non-BBH events together, with a true value of $f_{\rm nbh} = 1$, and (2) all the 16 BBH and 8 non-BBH events together, with $f_{\rm nbh} = 0.33$.

We estimate $f_{\rm nbh}$ for these two populations using the mixture-likelihood approach and find that the posteriors are consistent with the true values at very high confidences, as illustrated on the left panel of Fig. 6. The fact that we only had 8 and 24 events for these two populations has been reflective in the respective statistical uncertainties in Fig. 6 (left panel). This finding indicates that the bias in $f_{\rm nbh}$ primarily arises because our population contains many low-spin-low-SNR events.

B. Prior effects

Throughout the Bayesian inference, we have assumed the prior on $\delta\kappa_s$ as uniform in $[-500, 500]$. The injected populations, on the other hand, have $\delta\kappa_s$ drawn from narrower ranges with nonuniform distributions. Prior ranges that are wider than required will be penalized by Ocaam's factor. Below, we show that our prior choices can

---

[4]$\chi_{\rm eff}$ is the effective inspiral spin parameter captures the spin effects of nonprecessing binary system which is defined in terms of component masses m_i and dimensionless spins $\chi_i = \vec{S}_i \cdot \hat{L}/m_i^2$ as, $\chi_{\rm eff} = \frac{m_1\chi_1 + m_2\chi_2}{m_1 + m_2}$ [135].

partly account for the bias in $f_{\rm nbh}$ estimates. The right panel of Fig. 6 shows how the $f_{\rm nbh}$ posterior would change if we were to perform the analysis with the same prior as that of the injected $\delta\kappa_s$ distribution. In order to achieve this, we did a prior reweighting as described in Appendix. We have taken an example from our populations with $f_{\rm nbh} = 1$ and find that the posterior on $f_{\rm nbh}$ after prior reweighting (dashed curves) is closer to the true values.

Of course, in reality, we can not preacquire the knowledge of the underlying distribution. However, we can always assume a hyperparametrized prior model characterizing the underlying distribution and marginalize the likelihood over the hyperparameters to obtain the posteriors on $f_{\rm nbh}$. In Appendix, we have derived the formalism of performing this hyperparameter-marginalization though its detailed demonstration is differed for a future work.

C. Nonidentical nature of the binary components

Another possible, though minor, reason is our assumption of $\delta\kappa_a = 0$ (i.e., $\delta\kappa_1 = \delta\kappa_2$) in the analysis while our injections did not assume this. In other words, we have injected different values for $\delta\kappa_1$ and $\delta\kappa_2$ while in the Bayesian sampling, we assumed them to have equal values. This can lead to a bias in the estimated $\delta\kappa_s$ and the Bayes factor. Indeed, this is a prospect to explore in detail in a future study. Regardless of the $\delta\kappa_a = 0$ assumption, the posterior could capture the true value of $f_{\rm nbh}$, if the SNR and spins are high enough, as shown in the left panel of Fig. 6.

At higher detector sensitivity and with better waveform models such as those with higher modes [148–153], some further correlations between binary parameters are expected to break, leading to improved estimates of κ parameters and improved Bayes factors, for the individual events. This will eventually improve the measurement of $f_{\rm nbh}$.

VII. CONCLUSION AND FURTHER REMARKS

We have discussed how to effectively *combine* gravitational-wave data from multiple detections to probe subpopulations that include non-BH compact binaries. Our method is based on using spin-induced quadrupole moment as a physical parameter that distinguishes BBH from non-BBHs. We first analyzed the efficacy of the previously-employed hierarchical combining approach that relies on a Gaussian assumption for the population distribution of the spin-induced quadrupole moment parameter. Next, we introduced a mixture-likelihood approach (Sec. III C) that estimates the fraction (f_{nbh}) of non-BBH signals present in the observed population.

We simulated various populations that included BBH and non-BBH signals at different proportions. Our results show that both approaches are good for homogeneous populations like a BBH-only population. Also, both the approaches would signal if the population has complex nature with subpopulations being present. The mixture-likelihood approach is a natural choice to capture such complex distributions of non-BBH sub-populations. We applied the method on the LIGO-Virgo detected GW events from the GWTC-2 catalog and found them consistent with a BBH population.

Though the mixture-likelihood approach effectively rules out the BBH population hypothesis for the simulated populations that included some fraction of non-BBH signals, we notice that the method suffers from systematics in measuring the fraction of non-BBH signals precisely. We investigated possible reasons for these biases in Sec. VI. We find that the low values of the signal-to-noise ratios and intrinsic spins of the events in our population, and certain assumptions we made in the analysis prior (including the prior on $\delta\kappa_s$ parameter and the constraint that $\delta\kappa_a = 0$) could lead to the observed bias.

In the future, with more realistic astrophysical population models, our estimates may improve. This is anticipated primarily because the spin-induced quadrupole moment estimates from individual events and, hence, the population can change according to the intrinsic mass-spin distributions. Also, with more accurate waveform models being available, our measurements could further improve as they could help break some of the degeneracies that lead to the systematics in this study. We would also include the effect of selection bias in the inference of f_{nbh} which would allow redefining the *fraction* f_{nbh} as the fraction of non-BBH signals in the universe, rather than the fraction in the *observed* signals, in the future.

Finally, though we have demonstrated the mixture-likelihood approach using the measurement of spin-induced quadrupole moment parameters, the method is generic enough to include in or to be applied for the other physical parametrizations that distinguish BBH from non-BBH signals (as mentioned in Sec. I).

ACKNOWLEDGMENTS

APPENDIX: MARGINALIZING THE MIXTURE LIKELIHOOD OVER THE HYPERPARAMETERS OF $\delta\kappa_s$ DISTRIBUTION

In Eq. (16), we have considered a uniform prior on $\delta\kappa_s$ in estimating the evidence $\mathcal{Z}^{nbh}$. In a more generic treatment, we should hyperparametrize this prior and marginalize over, as the underlying $\delta\kappa_s$ distribution in the universe is unknown (See Ref. [155] for a comprehensive treatment of marginalizing over the prior hyperparameters, though in a different context). Thus, we first rewrite Eq. (16) with a generic prior on $\delta\kappa_s$, labeled as Λ. That means, Eq. (15) takes the form,

$$\mathcal{L}^{\mathrm{pop}}(\vec{d}|f_{\mathrm{nbh}},\Lambda) = \prod_{i=1}^{N}[(1-f_{\mathrm{nbh}})\mathcal{Z}_i^{bh} + f_{\mathrm{nbh}}\mathcal{Z}_i^{nbh}(\Lambda)], \quad \text{(A1)}$$

where $\mathcal{Z}_i^{nbh}(\Lambda)$ is the generalized version of Eq. (3),

$$\mathcal{Z}^{nbh}(\Lambda) = \int \pi(\vec{\theta},\delta\kappa_s|\Lambda)\mathcal{L}(d|\vec{\theta},\delta\kappa_s)d\vec{\theta}d\delta\kappa_s. \quad \text{(A2)}$$

The only difference being that the prior on $\delta\kappa_s$ is now informed by the hyperparameters Λ. Also, this hyperparameter space Λ could in general be a complex multidimensional parameter space. Perhaps, the simplest case one could consider is a zero-centered top-hat function, with only one parameter, namely λ. This would be a prior pretty

much like the one we have used in our analysis, $\pi(\delta\kappa_s|\lambda) \sim U(-\lambda, \lambda)$. Alternatively, if one assumes that all the non-BBH signals are from a certain class of exotic compact objects and have their $\delta\kappa_s$ distribution coming from a localized distribution, then a Gaussian with unknown mean and width would be a good representation, i.e., $\Lambda = \{\mu, \sigma^2\}$ Given a hyperparameter model, the corresponding evidence $\mathcal{Z}^{nbh}(\Lambda)$ at any given point in the Λ-space can be evaluated by re-weighting the prior, as discussed in Appendix A 1).

Once we have the tools to evaluate the likelihood, we can sample from the likelihood using any sampler, over the parameters, $\{f_{\mathrm{nbh}}, \Lambda\}$. This would give us the posterior probability density function as,

$$p(f_{\mathrm{nbh}}, \Lambda|d_{\mathrm{j}}) = \int \frac{\mathcal{L}^{pop}(d_{\mathrm{j}}|f_{\mathrm{nbh}}, \Lambda)\pi(f_{\mathrm{nbh}})\pi(\Lambda)}{\mathcal{Z}^{pop}_{\Lambda}}, \quad (A3)$$

with

$$\mathcal{Z}^{pop}_{\Lambda} = \int \mathcal{L}^{pop}(d_{\mathrm{j}}|f_{\mathrm{nbh}}, \Lambda)\pi(f_{\mathrm{nbh}})\pi(\Lambda)df_{\mathrm{nbh}}d\Lambda. \quad (A4)$$

Now we can obtain the posterior on f_{nbh} marginalized over Λ as,

$$p(f_{\mathrm{nbh}}|d_{\mathrm{j}}) = \int p(f_{\mathrm{nbh}}, \Lambda|d_{\mathrm{j}})d\Lambda. \quad (A5)$$

Employing a nested sampling algorithm for the sampling, from the likelihood given in Eq. (A2) the output will by default provide the probability of fraction defined in Eq. (A3). The priors on f_{nbh} and Λ can be taken as uniform. Given the posterior distribution on $\delta\kappa_s$, we can also reconstruct the population distribution of $\delta\kappa_s$ as,

$$p(\delta\kappa_s|d_{\mathrm{j}}) = \int p(\delta\kappa_s|\Lambda)p(\Lambda|d_{\mathrm{j}})d\Lambda. \quad (A6)$$

Equation (A6) is identical to Eq. (10) with the only visible difference being the hyperparameter vector $\vec{\alpha}$ replaced by Λ. The different notions of hyperparameters in Eq. (A6) and Eq. (10) are purposeful, while $\vec{\alpha}$ represents the distribution of $\delta\kappa_s$ from the entire population, Λ by definition represents the distribution of f_{nbh}, the fraction

of non-BBHs in the population. The remaining $(1 - f_{\mathrm{nbh}})$ fraction of sources have a delta function prior, given by $\delta(\delta\kappa_s - 0)$.

1. Evidence estimation by prior reweighting

Suppose we have the evidence estimated already assuming one prior, in our case a prior on $\delta\kappa_s$ assuming $U[-500, 500]$. Let us call this prior as Φ. Now the evidence for this prior $\mathcal{Z}^{nbh}(\Phi)$, according to the Bayes theorem, can be written as,

$$\mathcal{Z}^{nbh}(\Phi)p(\vec{\theta}, \delta\kappa_s|d_{\mathrm{j}}, \Phi) = \pi(\vec{\theta}, \delta\kappa_s|\Phi)\mathcal{L}(d_{\mathrm{j}}|\vec{\theta}, \delta\kappa_s), \quad (A7)$$

With the prior Λ, the new evidence will be as given by Eq. (A2). Plugging Eq. (A7) to Eq. (A2), we get

$$\mathcal{Z}^{nbh}(\Lambda) = \mathcal{Z}^{nbh}(\Phi) \int \frac{\pi(\vec{\theta}, \delta\kappa_s|\Lambda)}{\pi(\vec{\theta}, \delta\kappa_s|\Phi)} p(\vec{\theta}, \delta\kappa_s|d_{\mathrm{j}}, \Phi)d\vec{\theta}d\delta\kappa_s, \quad (A8)$$

where the probability distribution $p(\vec{\theta}, \delta\kappa_s|d_{\mathrm{j}}, \Phi)$ is known and the above integral can be approximated as a Monte-Carlo average over the posterior samples, i.e.,

$$\mathcal{Z}^{nbh}(\Lambda) = \mathcal{Z}^{nbh}(\Phi) \times \left[\frac{1}{n}\sum_{k=1}^{n} \frac{\pi(\vec{\theta}, \delta\kappa_s|\Lambda)}{\pi(\vec{\theta}, \delta\kappa_s|\Phi)}\right], \quad (A9)$$

where n is the number of samples in the $\delta\kappa_s$ posterior distribution. Both $\pi(\vec{\theta}, \delta\kappa_s|\Lambda)$ and $\pi(\vec{\theta}, \delta\kappa_s|\Phi)$ must be normalized distributions. Throughout the analysis, we assume that the priors on $\delta\kappa_s$ and $\vec{\theta}$ are uncorrelated and hence we can decouple $\pi(\vec{\theta})$ from both numerator and denominator so that they cancel each other. This leaves,

$$\mathcal{Z}^{nbh}(\Lambda) = \mathcal{Z}^{nbh}(\Phi) \times \left[\frac{1}{n}\sum_{k=1}^{n} \frac{\pi(\delta\kappa_s|\Lambda)}{\pi(\delta\kappa_s|\Phi)}\right], \quad (A10)$$

Equation (A10) makes it easier to compute the likelihood in Eq. (A1) for any instance of Λ. The reader may refer to Ref. [156] for a detailed treatment of the prior reweighting procedure.

---

[1] R. Abbott, T. Abbott, F. Acernese, K. Ackley, C. Adams, N. Adhikari, R. Adhikari, V. Adya, C. Affeldt, D. Agarwal *et al.*, arXiv:2111.03606 [Phys. Rev. X (to be published)].

[2] B. P. Abbott *et al.*, Phys. Rev. Lett. **116**, 061102 (2016).

[3] B. P. Abbott *et al.*, Phys. Rev. Lett. **116**, 241103 (2016).

[4] R. Abbott *et al.* (LIGO Scientific, Virgo Collaborations), Phys. Rev. X **11**, 021053 (2021).

[5] B. P. Abbott *et al.*, Phys. Rev. Lett. **118**, 221101 (2017).

[6] B. P. Abbott *et al.*, Astrophys. J. **851**, L35 (2017).

[7] B. P. Abbott *et al.*, Phys. Rev. Lett. **119**, 141101 (2017).

[8] B. P. Abbott *et al.* (LIGO Scientific, Virgo Collaborations), Phys. Rev. X **9**, 031040 (2019).

[9] R. Abbott *et al.* (LIGO Scientific, Virgo Collaborations), Phys. Rev. D **102**, 043015 (2020).

[10] R. Abbott *et al.* (LIGO Scientific, Virgo Collaborations), Astrophys. J. Lett. **896**, L44 (2020).

[11] R. Abbott *et al.* (LIGO Scientific, Virgo Collaborations), Phys. Rev. Lett. **125**, 101102 (2020).

[12] B. Abbott *et al.* (LIGO Scientific, Virgo Collaborations), Phys. Rev. Lett. **119**, 161101 (2017).

[13] B. Abbott *et al.* (LIGO Scientific, Virgo Collaborations), Astrophys. J. Lett. **892**, L3 (2020).

[14] R. Abbott *et al.* (LIGO Scientific, KAGRA, Virgo Collaborations), Astrophys. J. Lett. **915**, L5 (2021).

[15] A. H. Nitz, C. D. Capano, S. Kumar, Y.-F. Wang, S. Kastha, M. Schäfer, R. Dhurkunde, and M. Cabero, Astrophys. J. **922**, 76 (2021).

[16] A. H. Nitz, T. Dent, G. S. Davies, S. Kumar, C. D. Capano, I. Harry, S. Mozzon, L. Nuttall, A. Lundgren, and M. Tápai, Astrophys. J. **891**, 123 (2020).

[17] S. Olsen, T. Venumadhav, J. Mushkin, J. Roulet, B. Zackay, and M. Zaldarriaga, arXiv:2201.02252 [Phys. Rev. D (to be published)].

[18] J. Roulet, T. Venumadhav, B. Zackay, L. Dai, and M. Zaldarriaga, Phys. Rev. D **102**, 123022 (2020).

[19] V. Cardoso and P. Pani, arXiv:1904.05363.

[20] G. F. Giudice, M. McCullough, and A. Urbano, J. Cosmol. Astropart. Phys. 10 (2016) 001.

[21] P. Jetzer, Phys. Rep. **220**, 163 (1992).

[22] A. R. Liddle and M. S. Madsen, Int. J. Mod. Phys. D **01**, 101 (1992).

[23] F. E. Schunck and E. W. Mielke, Classical Quantum Gravity **20**, R301 (2003).

[24] S. L. Liebling and C. Palenzuela, Living Rev. Relativity **20**, 5 (2017).

[25] R. Brito, V. Cardoso, C. A. R. Herdeiro, and E. Radu, Phys. Lett. B **752**, 291 (2016).

[26] R. Friedberg, T. Lee, and Y. Pang, Phys. Rev. D **35**, 3640 (1987).

[27] R. Friedberg, T. Lee, and Y. Pang, Phys. Rev. D **35**, 3658 (1987).

[28] F. D. Ryan, Phys. Rev. D **55**, 6081 (1997).

[29] L. Visinelli and P. Gondolo, Phys. Rev. Lett. **113**, 011802 (2014).

[30] A. Bauswein, R. Oechslin, and H.-T. Janka, Phys. Rev. D **81**, 024012 (2010).

[31] D. Gondek-Rosinska and F. Limousin, arXiv:0801.4829.

[32] F. Weber, Prog. Part. Nucl. Phys. **54**, 193 (2005).

[33] J. Madsen, Lect. Notes Phys. **516**, 162 (1999).

[34] C. Alcock, E. Farhi, and A. Olinto, Astrophys. J. **310**, 261 (1986).

[35] M. G. Alford, Annu. Rev. Nucl. Part. Sci. **51**, 131 (2001).

[36] C. Kouvaris and N. G. Nielsen, Phys. Rev. D **92**, 063526 (2015).

[37] K. Freese, T. Rindler-Daller, D. Spolyar, and M. Valluri, Rep. Prog. Phys. **79**, 066902 (2016).

[38] C. Chirenti and L. Rezzolla, Phys. Rev. D **94**, 084016 (2016).

[39] C. B. M. H. Chirenti and L. Rezzolla, Classical Quantum Gravity **24**, 4191 (2007).

[40] F. S. Lobo, Classical Quantum Gravity **23**, 1525 (2006).

[41] B. M. Carter, Classical Quantum Gravity **22**, 4551 (2005).

[42] M. Visser and D. L. Wiltshire, Classical Quantum Gravity **21**, 1135 (2004).

[43] P. O. Mazur and E. Mottola, arXiv:gr-qc/0109035.

[44] S. Tulin, H.-B. Yu, and K. M. Zurek, Phys. Rev. D **87**, 115007 (2013).

[45] G. Bertone *et al.*, SciPost Phys. Core **3**, 007 (2020).

[46] L. Barack *et al.*, Classical Quantum Gravity **36**, 143001 (2019).

[47] F. Ferrer, A. M. da Rosa, and C. M. Will, Phys. Rev. D **96**, 083014 (2017).

[48] D. Spolyar, K. Freese, and P. Gondolo, Phys. Rev. Lett. **100**, 051101 (2008).

[49] N. V. Krishnendu, K. G. Arun, and C. K. Mishra, Phys. Rev. Lett. **119**, 091101 (2017).

[50] V. Cardoso, E. Franzin, A. Maselli, P. Pani, and G. Raposo, Phys. Rev. D **95**, 084014 (2017); **95**, 089901(A) (2017).

[51] N. Sennett, T. Hinderer, J. Steinhoff, A. Buonanno, and S. Ossokine, Phys. Rev. D **96**, 024002 (2017).

[52] N. K. Johnson-Mcdaniel, A. Mukherjee, R. Kashyap, P. Ajith, W. Del Pozzo, and S. Vitale, Phys. Rev. D **102**, 123010 (2020).

[53] B. Abbott *et al.* (KAGRA, LIGO Scientific, Virgo Collaborations), Living Rev. Relativity **21**, 3 (2018).

[54] J. Aasi *et al.* (The LIGO Scientific Collaboration), Classical Quantum Gravity **32**, 074001 (2015).

[55] F. Acernese *et al.* (Virgo Collaboration), Classical Quantum Gravity **32**, 024001 (2015).

[56] T. Venumadhav, B. Zackay, J. Roulet, L. Dai, and M. Zaldarriaga, Phys. Rev. D **101**, 083030 (2020).

[57] B. Sathyaprakash *et al.*, in *Proceedings, 46th Rencontres de Moriond on Gravitational Waves and Experimental Gravity: La Thuile, Italy, March 20-27, 2011* (2011), pp. 127–136, arXiv:1108.1423.

[58] T. Regimbau *et al.*, Phys. Rev. D **86**, 122001 (2012).

[59] S. Hild *et al.*, Classical Quantum Gravity **28**, 094013 (2011).

[60] S. Hild, S. Chelkowski, and A. Freise, arXiv:0810.0604.

[61] B. P. Abbott *et al.* (LIGO Scientific Collaboration), Classical Quantum Gravity **34**, 044001 (2017).

[62] M. Ando *et al.*, Classical Quantum Gravity **26**, 094019 (2009).

[63] LISA Pathfinder Collaboration, J. Phys. **840**, 012001 (2017).

[64] M. Armano *et al.*, Phys. Rev. Lett. **116**, 231101 (2016).

[65] M. Armano *et al.*, arXiv:1903.08924.

[66] N. V. Krishnendu, M. Saleem, A. Samajdar, K. G. Arun, W. Del Pozzo, and C. K. Mishra, Phys. Rev. D **100**, 104019 (2019).

[67] F. D. Ryan, Phys. Rev. D **52**, 5707 (1995).

[68] N. A. Collins and S. A. Hughes, Phys. Rev. D **69**, 124022 (2004).

[69] S. J. Vigeland and S. A. Hughes, Phys. Rev. D **81**, 024030 (2010).

[70] K. Glampedakis and S. Babak, Classical Quantum Gravity **23**, 4167 (2006).

[71] X. Jiménez Forteza, T. Abdelsalhin, P. Pani, and L. Gualtieri, Phys. Rev. D **98**, 124014 (2018).

[72] T. Abdelsalhin, L. Gualtieri, and P. Pani, Phys. Rev. D **98**, 104046 (2018).

[73] R. A. Porto, Fortschr. Phys. **64**, 723 (2016).

[74] E. Berti and V. Cardoso, Int. J. Mod. Phys. D **15**, 2209 (2006).

[75] C. F. B. Macedo, P. Pani, V. Cardoso, and L. C. B. Crispino, Phys. Rev. D **88**, 064046 (2013).

[76] C. F. B. Macedo, V. Cardoso, L. C. B. Crispino, and P. Pani, Phys. Rev. D **93**, 064053 (2016).

[77] S. Gossan, J. Veitch, and B. S. Sathyaprakash, Phys. Rev. D **85**, 124056 (2012).

[78] T. Binnington and E. Poisson, Phys. Rev. D **80**, 084018 (2009).

[79] N. Gürlebeck, Phys. Rev. Lett. **114**, 151102 (2015).

[80] T. Damour and A. Nagar, Phys. Rev. D **80**, 084035 (2009).

[81] T. Hinderer, Astrophys. J. **677**, 1216 (2008).

[82] É. É. Flanagan and T. Hinderer, Phys. Rev. D **77**, 021502 (2008).

[83] P. Pani, L. Gualtieri, A. Maselli, and V. Ferrari, Phys. Rev. D **92**, 024010 (2015).

[84] J. B. Hartle, Phys. Rev. D **8**, 1010 (1973).

[85] A. Maselli, P. Pani, V. Cardoso, T. Abdelsalhin, L. Gualtieri, and V. Ferrari, Phys. Rev. Lett. **120**, 081101 (2018).

[86] K. Chatziioannou, E. Poisson, and N. Yunes, Phys. Rev. D **94**, 084043 (2016).

[87] K. Chatziioannou, E. Poisson, and N. Yunes, Phys. Rev. D **87**, 044022 (2013).

[88] W. G. Laarakkers and E. Poisson, Astrophys. J. **512**, 282 (1999).

[89] G. Pappas and T. A. Apostolatos, arXiv:1211.6299.

[90] G. Pappas and T. A. Apostolatos, Phys. Rev. Lett. **108**, 231104 (2012).

[91] T. Narikawa, N. Uchikata, and T. Tanaka, Phys. Rev. D **104**, 084056 (2021).

[92] L. Blanchet, Living Rev. Relativity **9**, 4 (2006).

[93] S. Marsat, A. Bohé, G. Faye, and L. Blanchet, Classical Quantum Gravity **30**, 055007 (2013).

[94] A. Bohé, S. Marsat, G. Faye, and L. Blanchet, Classical Quantum Gravity **30**, 075017 (2013).

[95] A. Bohé, S. Marsat, and L. Blanchet, Classical Quantum Gravity **30**, 135009 (2013).

[96] S. Marsat, A. Bohé, L. Blanchet, and A. Buonanno, Classical Quantum Gravity **31**, 025023 (2014).

[97] A. Bohé, G. Faye, S. Marsat, and E. K. Porter, Classical Quantum Gravity **32**, 195010 (2015).

[98] S. Marsat, Classical Quantum Gravity **32**, 085008 (2015).

[99] K. G. Arun, A. Buonanno, G. Faye, and E. Ochsner, Phys. Rev. D **79**, 104023 (2009); **84**, 049901(E) (2011).

[100] L. E. Kidder, Phys. Rev. D **52**, 821 (1995).

[101] C. M. Will and A. G. Wiseman, Phys. Rev. D **54**, 4813 (1996).

[102] A. Buonanno, G. Faye, and T. Hinderer, Phys. Rev. D **87**, 044009 (2013).

[103] L. Blanchet, Living Rev. Relativity **17**, 2 (2014).

[104] C. K. Mishra, A. Kela, K. G. Arun, and G. Faye, Phys. Rev. D **93**, 084054 (2016).

[105] A. Buonanno and T. Damour, Phys. Rev. D **59**, 084006 (1999).

[106] A. Nagar *et al.*, Phys. Rev. D **98**, 104052 (2018).

[107] Y. Pan, A. Buonanno, A. Taracchini, L. E. Kidder, A. H. Mroué, H. P. Pfeiffer, M. A. Scheel, and B. Szilágyi, Phys. Rev. D **89**, 084006 (2014).

[108] L. Blanchet, Living Rev. Relativity **17**, 2 (2014).

[109] F. Pretorius, Phys. Rev. Lett. **95**, 121101 (2005).

[110] M. Sasaki and H. Tagoshi, Living Rev. Relativity **6**, 6 (2003).

[111] M. Sasaki and H. Tagoshi, Living Rev. Relativity **6**, 6 (2003).

[112] T. Dietrich *et al.*, Phys. Rev. D **99**, 024029 (2019).

[113] J. E. Thompson, E. Fauchon-Jones, S. Khan, E. Nitoglia, F. Pannarale, T. Dietrich, and M. Hannam, Phys. Rev. D **101**, 124059 (2020).

[114] T. Dietrich, S. Bernuzzi, and W. Tichy, Phys. Rev. D **96**, 121501 (2017).

[115] V. Cardoso and P. Pani, Living Rev. Relativity **22**, 4 (2019).

[116] C. Pacilio, M. Vaglio, A. Maselli, and P. Pani, Phys. Rev. D **102**, 083002 (2020).

[117] J. Balakrishna, R. Bondarescu, G. Daues, F. Siddhartha Guzman, and E. Seidel, Classical Quantum Gravity **23**, 2631 (2006).

[118] J. Abedi, H. Dykaar, and N. Afshordi, Phys. Rev. D **96**, 082004 (2017).

[119] B. P. Abbott *et al.* (LIGO Scientific, Virgo Collaborations), Classical Quantum Gravity **37**, 045006 (2020).

[120] T. Abdelsalhin, Other thesis, 2019, arXiv:1905.00408.

[121] K. Huang, J. Hu, Y. Zhang, and H. Shen, Astrophys. J. **904**, 39 (2020).

[122] S. Datta, K. S. Phukon, and S. Bose, Phys. Rev. D **104**, 084006 (2021).

[123] V. Cardoso and P. Pani, Nat. Astron. **1**, 586 (2017).

[124] N. Krishnendu and A. B. Yelikar, Classical Quantum Gravity **37**, 205019 (2020).

[125] R. O. Hansen, J. Math. Phys. (N.Y.) **15**, 46 (1974).

[126] B. Carter, Phys. Rev. Lett. **26**, 331 (1971).

[127] N. Gürlebeck, Phys. Rev. Lett. **114**, 151102 (2015).

[128] R. Abbott *et al.* (LIGO Scientific, Virgo Collaborations), arXiv:2010.14529.

[129] M. Isi, K. Chatziioannou, and W. M. Farr, Phys. Rev. Lett. **123**, 121101 (2019).

[130] R. Abbott *et al.* (LIGO Scientific, Virgo Collaborations), Phys. Rev. D **103**, 122002 (2021).

[131] E. Poisson, Phys. Rev. D **57**, 5287 (1998).

[132] P. O. Mazur and E. Mottola, Proc. Natl. Acad. Sci. U.S.A. **101**, 9545 (2004).

[133] N. Uchikata and S. Yoshida, Classical Quantum Gravity **33**, 025005 (2016).

[134] N. Uchikata, S. Yoshida, and P. Pani, Phys. Rev. D **94**, 064015 (2016).

[135] P. Ajith *et al.*, Phys. Rev. Lett. **106**, 241101 (2011).

[136] S. Husa, S. Khan, M. Hannam, M. Pürrer, F. Ohme, X. Jiménez Forteza, and A. Bohé, Phys. Rev. D **93**, 044006 (2016).

[137] M. Hannam, P. Schmidt, A. Bohé, L. Haegel, S. Husa, F. Ohme, G. Pratten, and M. Pürrer, Phys. Rev. Lett. **113**, 151101 (2014).

[138] N. V. Krishnendu, C. K. Mishra, and K. G. Arun, Phys. Rev. D **99**, 064008 (2019).

[139] J. Veitch *et al.*, Phys. Rev. D **91**, 042003 (2015).

[140] R. Smith and E. Thrane, Phys. Rev. X **8**, 021019 (2018).

[141] B. Abbott *et al.* (LIGO Scientific, Virgo Collaborations), Astrophys. J. Lett. **882**, L24 (2019).

[142] R. Abbott *et al.* (LIGO Scientific, Virgo Collaborations), Astrophys. J. Lett. **913**, L7 (2021).

[143] LIGO Scientific Collaboration, https://dcc.ligo.org/LIGO-M060056/public (2009).

[144] LIGO Scientific Collaboration, https://www.advancedligo.mit.edu/ (2018).

[145] F. Acernese *et al.*, Classical Quantum Gravity **23**, S635 (2006).

[146] LIGO Scientific Collaboration, LIGO Algorithm Library—LALSuite, free software (GPL) (2018).

[147] LIGO Scientific and Virgo Collaborations, GWTC-2, 10.7935/82H3-HH23 (2018).

[148] F. H. Shaik, J. Lange, S. E. Field, R. O'Shaughnessy, V. Varma, L. E. Kidder, H. P. Pfeiffer, and D. Wysocki, Phys. Rev. D **101**, 124054 (2020).

[149] V. Varma and P. Ajith, Phys. Rev. D **96**, 124024 (2017).

[150] J. Calderón Bustillo, S. Husa, A. M. Sintes, and M. Pürrer, Phys. Rev. D **93**, 084019 (2016).

[151] C. Capano, Y. Pan, and A. Buonanno, Phys. Rev. D **89**, 102003 (2014).

[152] T. B. Littenberg, J. G. Baker, A. Buonanno, and B. J. Kelly, Phys. Rev. D **87**, 104003 (2013).

[153] C. Kalaghatgi, M. Hannam, and V. Raymond, Phys. Rev. D **101**, 103004 (2020).

[154] https://www.gw-openscience.org

[155] R. J. E. Smith, C. Talbot, F. Hernandez Vivanco, and E. Thrane, Mon. Not. R. Astron. Soc. **496**, 3281 (2020),

[156] E. Thrane and C. Talbot, Pub. Astron. Soc. Aust. **36**, e010 (2019).